A review of aeronautical fatigue investigations in Sweden during the period May 2003 to May 2005

Presented at the 29th Conference of the International Committee on Aeronautical Fatigue Hamburg, Germany, 6-7 June 2005

EDITOR: ANDERS F. BLOM

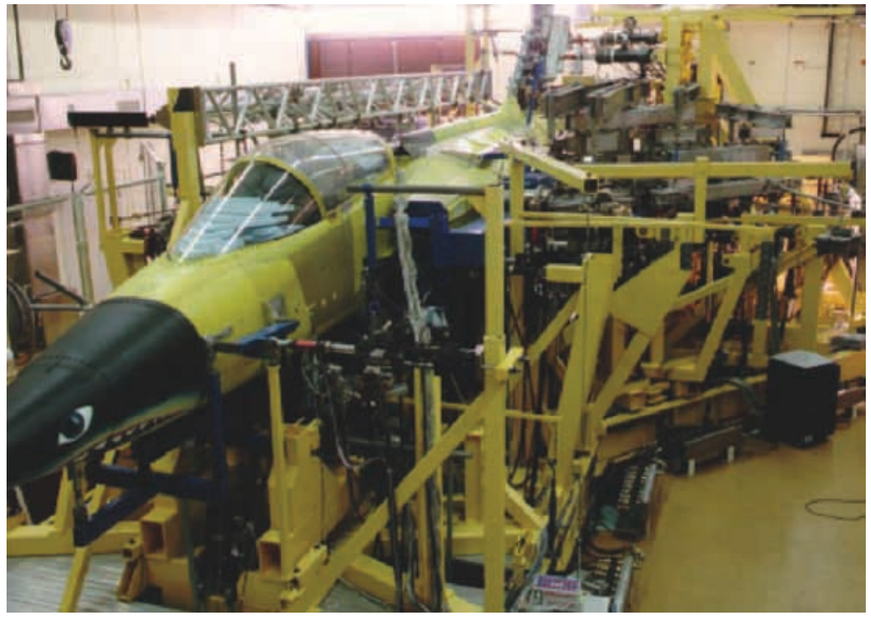

FOI is an assignment-based authority under the Ministry of Defence. The core activities are research, method and technology development, as well as studies for the use of defence and security. The organization employs around 1350 people of whom around 950 are researchers. This makes FOI the largest research institute in Sweden. FOI provides its customers with leading expertise in a large number of fields such as security-policy studies and analyses in defence and security, assessment of different types of threats, systems for control and management of crises, protection against and management of hazardous substances, IT-security an the potential of new sensors.

FOI
Defence Research Agency
Systems Technology
SE-164 90

Phone: +46 8-5550 3000
Fax: +46 8:5550 3100

www.foi.se

FOI-R-- 1646 --SE Scientific report
ISSN 1650-1942 June 2005

Systems Technology

A review of aeronautical fatigue investigations in Sweden during the period May 2003 to May 2005

Presented at the 29th Conference of the International Committee on Aeronautical Fatigue
Hamburg, Germany, 6-7 June 2005

FOI-R--1646--SE
ISSN 1650-1942

Systems Technology
Scientific report

June 2005

Issuing organization FOI – Swedish Defence Research Agency Systems Technology SE-164 90 Stockholm	**Report number, ISRN** FOI-R--1646--SE	**Report type** Scientific report
	Research area code 7. Mobility and space technology, incl materials	
	Month year June 2005	**Project no.** I6011
	Sub area code 73 Air vehicle technology	
	Sub area code 2	
Author/s (editor/s) Editor: Anders F. Blom	**Project manager**	
	Approved by Monica Dahlén	
	Sponsoring agency FOI, US Air Force	
	Scientifically and technically responsible Anders F. Blom	

Report title

A review of aeronautical fatigue investigations in Sweden during the period May 2003 to May 2005

Abstract (not more than 200 words)

In this paper a review is given of the work carried out in Sweden in the area of aeronautical fatigue during the period May 2003 to May 2005. The review includes basic studies of fatigue development in metals, stress analysis and fracture mechanics, studies of crack propagation and residual strength, and testing of full-scale structures. A reference list of relevant papers issued during the period covered by the review is included.

Keywords

Full scale testing, load spectra, metal fatigue, stress analysis, fracture mechanics crack propagation, residual strength

Further bibliographic information	**Language** English
ISSN 1650-1942	**Pages** 32 p.
	Price acc. to pricelist

Utgivare FOI - Totalförsvarets forskningsinstitut Systemteknik 164 90 Stockholm	**Rapportnummer, ISRN** FOI-R--1646--SE	**Klassificering** Vetenskaplig rapport
	Forskningsområde 7. Farkost- och rymdteknik, inkl material	
	Månad, år Juni 2005	**Projektnummer** I6011
	Delområde 73 Flygfarkostteknik	
	Delområde 2	
Författare/redaktör Editor: Anders F. Blom	**Projektledare**	
	Godkänd av Monica Dahlén	
	Uppdragsgivare/kundbeteckning FOI, US Air Force	
	Tekniskt och/eller vetenskapligt ansvarig Anders F. Blom	
Rapportens titel (i översättning) Sammanfattning av aeronautiska utmattningsundersökningar i Sverige under perioden maj 2003 till maj 2005		

Sammanfattning (högst 200 ord)

I denna rapport presenteras en sammanställning av arbeten utförda i Sverige inom området flygteknisk utmattning under perioden maj 2003 till maj 2005. Sammanställningen innehåller grundläggande studier avseende utmattning i metaller, spänningsanalys och brottmekanik, studier av sprickpropagering och resthållfasthet, samt provning av strukturer i full skala. En referenslista avseende relevanta artiklar som utgivits under perioden som sammanställningen avser är inkluderad.

Nyckelord

Fullskaleprovning, lastspektra, metallutmattning, spänningsanalys, brottmekanik, spricktillväxt, resthållfasthet

Övriga bibliografiska uppgifter	**Språk** Engelska
ISSN 1650-1942	**Antal sidor:** 32 s.
Distribution enligt missiv	**Pris: Enligt prislista**

CONTENTS

3.1 INTRODUCTION

In this paper a review is given of the work carried out in Sweden in the area of aeronautical fatigue during the period May 2003 to May 2005. The review includes basic studies of fatigue development in metals, stress analysis and fracture mechanics, studies of crack propagation and residual strength, and testing of full-scale structures. A reference list of relevant papers issued during the period covered by the review is included.

Contributions to the present review are from the following sources:

– The Swedish Defence Research Agency (FOI), Systems Technology
  Sections 3.3.1, 3.3.2, 3.3.3, and 3.4.1

– The SAAB Company
  Sections 3.2.1, 3.2.2, 3.2.3, and 3.2.4

3.2 STRUCTURAL EVALUATION

3.2.1 The Saab 340 Full Scale Fatigue Test

General

The Design Service Goal (DSG) for Saab 340 is presently 90000 flights or 45000 flight hours whichever occurs first. However, an authorized Service Life Extension Program allows the operators to extend the utilization to 60000 flight hours (after embodiment of subject Service Bulletins)

The Saab 340 Full Scale Fatigue test has been tested for 204000 simulated flights. Thereby, the cyclic testing of the airframe is completed. The first 180000 flights of the testing finalized the fatigue phase of the test. Consequently, the Design Service Goal (DSG) of 90000 flights has been verified using a scatter factor of two. Artificial damages were embodied after the fatigue testing in order to verify the damage tolerance characteristics of the airframe structure. This damage tolerance phase of testing with artificial notches has been completed and accordingly 24000 flights have been simulated. Thus, the longest inspection interval (12000 flights) outlined in the Maintenance Review Board Report has been verified with a scatter factor of 2. Subsequently, the Saab 340 airframe was subjected to a numerous residual static strength test in order to verify requirements of large crack capability.

Damage Tolerance phase

The damage tolerance testing was conducted to verify the possible crack propagation and verify the damage tolerance analysis of SAAB 340 in accordance with requirements presented in FAR/EASA 25.571. The subject testing was also used for verification of the predefined inspection program given in the mandatory maintenance program.

A total of 24 artificial damages were introduced before start of damage tolerance testing. The test specimen was subjected to fatigue testing for 24,000 flights. The damages can be divided into two different types:

- Damages where the intention is to study the crack growth rate.
- Damages in fail safe structure, where the primary load path is removed. In this case the ”residual fatigue life” of the remaining load paths, i.e. the time to initiation of secondary cracks, is of interest. The subsequent crack growth rate of possible secondary cracks will also be studied.

The following structural parts have been furnished with artificial damages:

- Wing: lower panels, lower spar caps, front and rear spar web, wing centre splice, wing to fuselage attachment.
- Fuselage: skin panels, skin splices, skin cut-outs
- Cockpit: pilot window posts
- Stabiliser: stabiliser spar/skin, stabiliser/fuselage attachment.
- Nacelle: upper longeron

The selected damages were considered to cover the relevant types of spectra, crack types and materials, in order to justify the complete damage tolerance verification of the Saab 340.

The experiences from the damage tolerance testing have been taken into consideration in the damage tolerance verification and accordingly the existing in service inspection program has been updated if required.

The damage tolerance testing have experienced that it is sometimes difficult to observe any natural crack propagation of artificial flaws or notches. The theoretical crack growth analysis indicates a portion of conservatism for the analysed crack propagation.

Residual strength test phase

The static residual strength test program has been terminated implying that the entire airframe was tested for 25 static limit load cases in order to verify the structure for predetermined critical crack length conditions.

Primary structural elements such as circumferential /longitudinal fuselage splices, wing spars and horizontal stabilizer spars were accordingly subjected to the most critical load case up to limit load level. Figure 1 to 2 outlines some examples of the location and nature of the artificial cracks exposed to the residual strength tests.

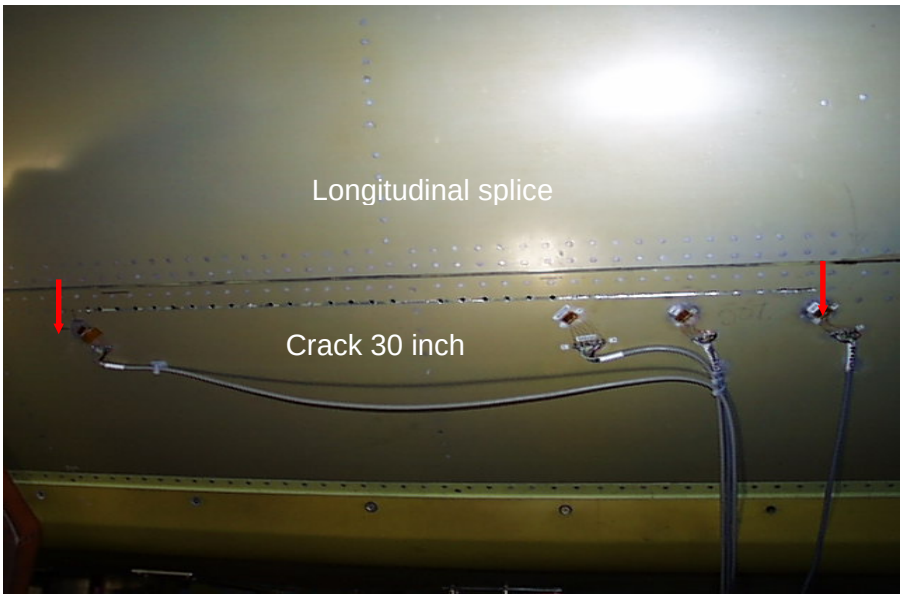

Figure 1. Saab 340 Fuselage- Residual Strength test of longitudinal splice.

Accidental damages such creases and major dents were also tested during the residual strength test program aiming to verify the impact of such damages. Areas like stabilizer panels door elements, fuselage panels prone to ground handling damages were subjected various static load tests.

All the residual static tests were carried out up to limit load level with successful results. On the bases of these results it was thereby demonstrated that the Saab 340 airframe fulfil all civil requirements (FAR/EASA regulations) of residual strength capability.

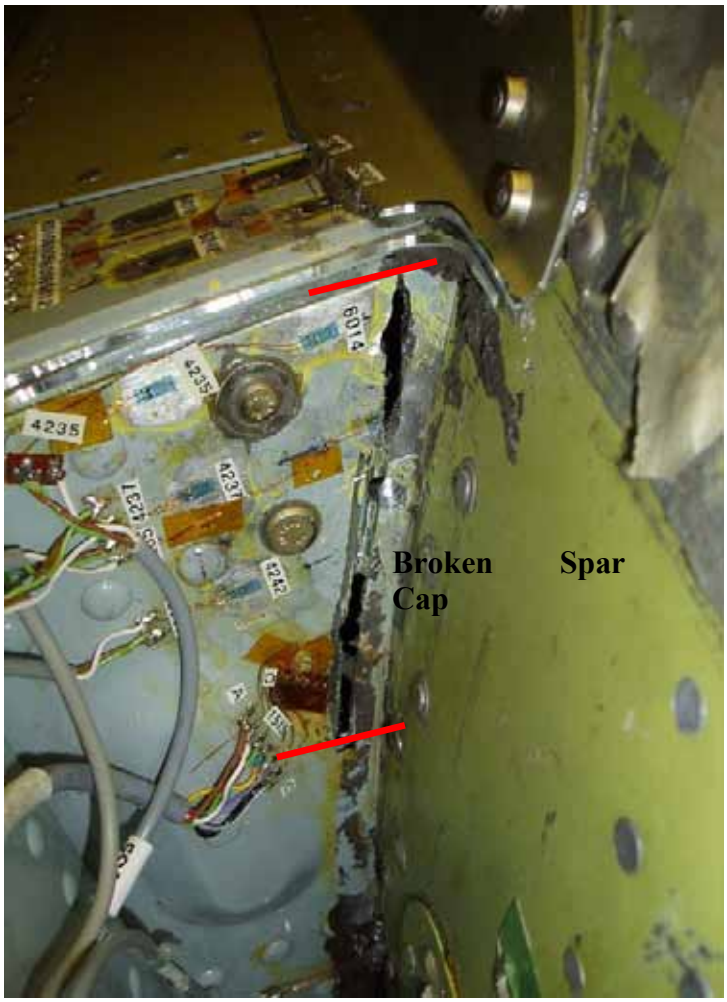

Figure 2. Saab 340 Fuselage- Residual Strength Test of the forward horizontal spar.

3.2.2 Saab 2000 Full Scale Fatigue Test

General

The Design Service Goal (DSG) for Saab 2000 is presently 75000 flights or 60000 flight hours whichever occurs first. For the Saab 2000, no complete airframe will be tested due to the commonality with the Saab 340. Consequently, a number of full scale component tests are used to justify the long tem characteristics.

Empennage structure, fatigue and damage tolerance test

This test included the horizontal stabilisers and the attachment structure to the rear fuselage.

The fatigue phase including the damage tolerance test is completed, comprising of 150000 flights in pure fatigue test with subsequent testing with artificial notches for further 24000 flights.

A total number of four artificial damages were inflicted on the test specimen. These artificial damages can be classified into two types as follows:

- Damages where the intention is to study the crack growth rate.
- Damages in fail safe structure, where the primary load path is removed. In this case the ”residual fatigue life” of the remaining load paths, i.e. the time to initiation of secondary cracks, is of interest. The subsequent crack growth rate of possible secondary cracks will also be studied.

The following structural elements of the horizontal stabiliser have been subjected to artificial cracks. This was made by mechanical means in terms of sawing, grinding or cutting.

- Stabiliser/fuselage attachment
  Study of crack growth rate for a crack in the stabiliser spar cap, from a fastener hole at the attachment to the fuselage frame.
- Rear spar web
  Study of crack growth rate for a crack growing from an inspection hole.
- Upper skin panel
  Study of crack growth rate for a crack growing from a fastener hole towards the honey comb core.
- Mid hinge
  Study of crack growth rate for a crack growing from a fastener hole (LHS), study of residual fatigue life and crack growth of possible secondary cracks after complete failure of one of two parts in the mid hinge (RHS).

The rationale for selecting the aforementioned damages is that the damages shall cover relevant types of spectra, crack types and materials in order to constitute a substantiation of the damage tolerance analysis of the Saab 2000 horizontal stabilisers.

The experiences from the damage tolerance testing have been taken into consideration in the damage tolerance verification and if necessary the existing in service inspection program has been updated to reflect the results from the testing.

Residual strength tests have taken place to show compliance with the FAR/EASA requirements with respect to residual strength evaluation. This implies that the remaining structure must be able to withstand an arbitrary limit load condition.

The horizontal stabilizer was tested with four critical artificial saw cuts located at the most critical location of the principal structural elements.

Primary spars, critical sections of the panel and attachment to fuselage were provided artificial saw cuts corresponding to critical sizes per the theoretical analysis.

Figure 3 outlines the artificial saw cut at the inboard section where the main spar is attached to the fuselage frame.

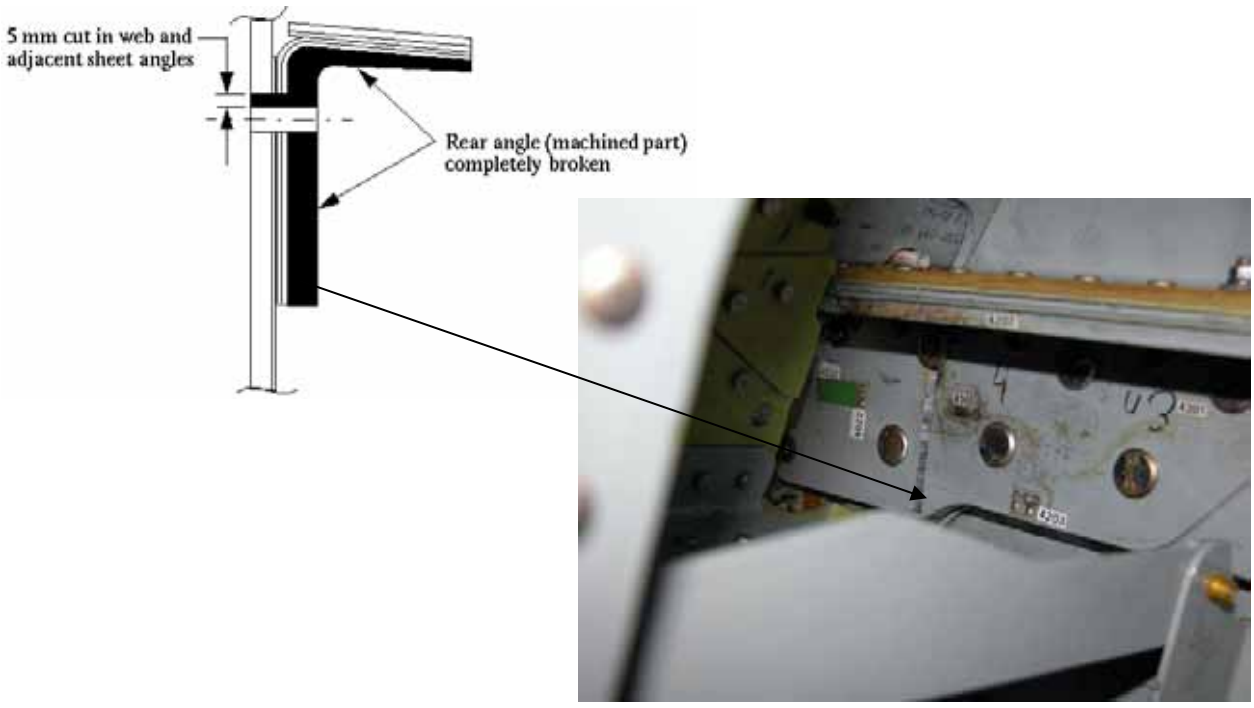

Figure 3. Saab 2000 Residual strength test- artificial saw cut at the inboard section of the horizontal stabilizer.

The residual static tests were carried out up to at least limit load level with satisfactory results. Based on these results, it was thereby demonstrated that the empennage structure to the Saab 2000 fulfil all civil requirements (FAR/EASA regulations) of residual strength capability.

Subsequently, accidental damages in terms of multiple and major dents were also tested during a separate residual strength test. All saw cuts except the saw cut at the inboard section were repaired prior to this final test. The lower skin panel was provided with multiple dents simulating inappropriate maintenance on aircraft in service.

Figure 4 depicts the distribution of the multiple dents in the panel. The test specimen was loaded to 178 % of the limit load level before test was interrupted due to limitations in the loading system. The test specimen maintained the structural integrity at this high load level, no discrepancies were noted in the spar interface or at zone for the artificial dents per figure 4.

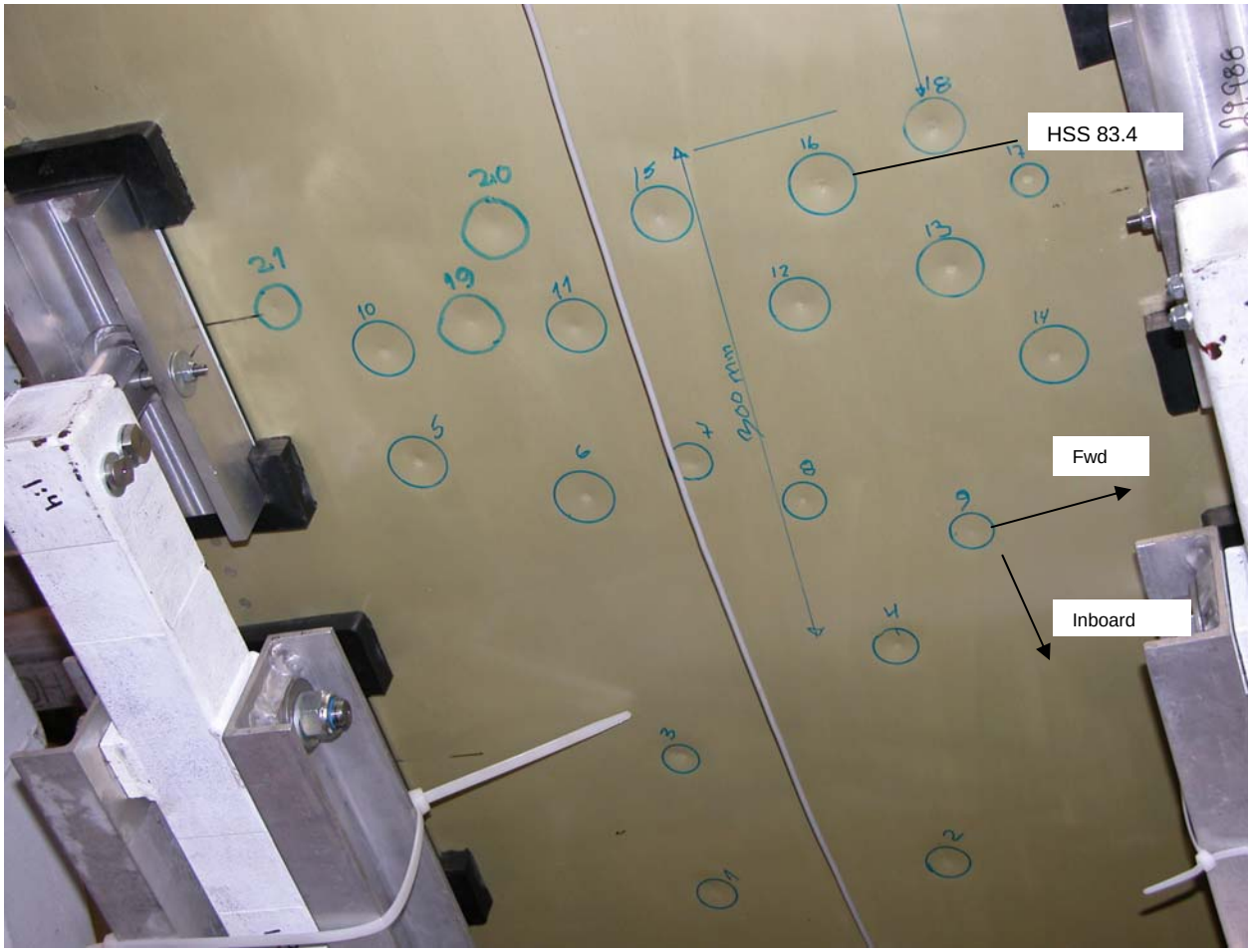

Figure 4. Saab 2000 Residual strength test- 178 % limit load level simulating accidental damages.

Wing/fuselage fatigue test

The subject test includes the centre and the rear part of the fuselage, the complete wing torque box and the rear part of the engine nacelles.

The wing detail design is changed compared to the Saab 340 (machined spars with integral spar caps), and the wing/fuselage interface also. Furthermore the cabin pressurisation spectrum is more severe, more exactly twice as severe as the spectra for the Saab 340 aircraft. The flight and landing loads on the fuselage is also more severe due to the slender fuselage of Saab 2000.

The first part of Wing/Fuselage Fatigue test up to 150000 flights with fatigue loads is finalised. Subsequently, the damage tolerance testing will continue aiming to reach 2'12000 flights with artificial notches.

Twenty five different types of damages have been defined reflecting the damage tolerance characteristics of various principal structural elements of the Saab 2000 airframe.

In conformity with all other tests, the wing/fuselage structure will be tested to demonstrate the damage tolerance characteristics in accordance with airworthiness requirements specified in FAR/EASA regulations. This also includes residual strength tests up to limit load condition for selected and critical load cases.

Prior to commencing the test, a revised and a lesser truncated sequence need to be defined.

Due to some findings, a limited number of areas on the wing structure have been subjected to cold working in order to improve the economical life of the wing spars and skins. Hence, a retrofit Service Bulletin is called out to enhance the fatigue characteristics and consequently avoid future time and cost consuming repairs.

Engine Mount structure fatigue test

The Saab 2000 engine mounting structure is completely different in design compared to the Saab 340. Eighth steel struts attaching to the forward engine mounts to the nacelle structure basically build up the structure. Each of those eight struts is redundant in terms of continuing airworthiness if an arbitrary strut is failed.

The fatigue phase of the test is completed (verification of 150000 flights from fatigue point of view). A number of fail safe situations (simulating a broken strut or fitting) with respect to the fatigue behaviour are tested in order to check the fail safe characteristics of the entire trussgrid under the fatigue loading. This portion of the test verified the fail-safe concept for a time period of 3*12000 flights.

The damage tolerance phase with artificial cracks will be final phase of this test programme.

3.2.3 JAS39 Gripen Fatigue Testing

The strength verification programme with large components was completed during 1994. The full scale fatigue test of the twin seater, 39B, was completed in 2000. The full scale fatigue test of the single seater, 39A, is still running and the full scale fatigue test of the twin seater export version, 39D, has begun.

Full scale fatigue test of the single seater, 39A

The configuration of the major fatigue test is almost identical to that of the major static test, both with regard to the structure and the test arrangement, figure 5. The test set-up has about 90 control channels, more than 1,000 strain gauges installations and is monitored by acoustic emission, besides the inspection by conventional methods.

The initial aim to verify a service life of 4,000 hours (5,600 flights) by flight simulation testing to 16,000 hours (22,400 flights) was completed in 1999. No cracks were detected during and after the testing except in parts belonging to the air brakes.

The objectives with testing beyond 16,000 hours, with the aim to reach 32,000 hours, are to verify wing and fin structure for the C and D versions of the aircraft. Another secondary goal is to identify areas in the fuselage where fatigue, in the long run, may show up in the A and B versions. The test has today (May 2005) been subjected beyond 26,000 hours (37,800 flights). Between 16,000 hours and 26,000 hours have a few cracks been found:

- in a lug for the attachment of the actuator for the main landing gear door.
- at hole edges in webs of formed sheet frames.
- at tool holes in the web of a machined fin attachment frame.

The outcome of the test has been used to retrofit operational aircraft and to redesign parts for the C and D versions for the Swedish airforce as well as for export aircraft. The lug for the main landing gear door actuator and the parts for the airbrake are redesigned. The formed sheet frames are replaced by high speed machined integral frames and the web of the machined fin attachment frame is made thicker. The cracking is not a flight safety issue but the rectifying actions have been made in order to avoid any cracking at all during the design life.

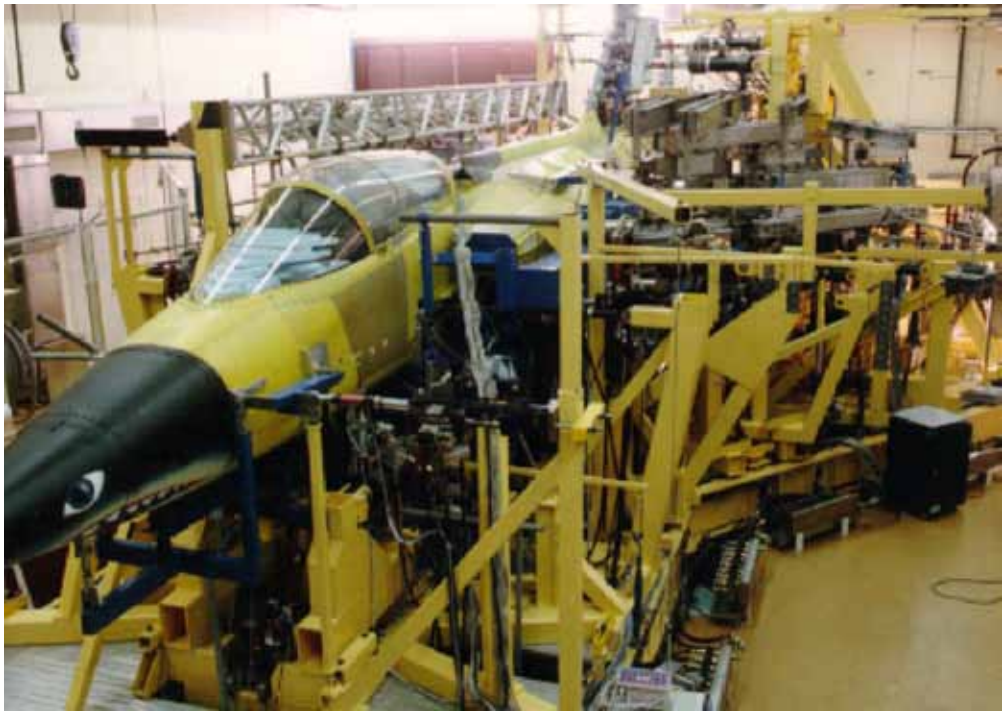

Figure 5. Photograph of the full scale fatigue test of the Gripen single seater, 39A.

Full scale fatigue test of the twin seater export version, 39D

The test object is a complete fuselage, figure 6 and 7. Attachment loads from the wings, fin, foreplanes, landing gears etc. are applied via dummies. The whole test set-up has about 90 control channels (actuators and pressure valves) and the structure is equipped with more than 1,000 strain gauges.

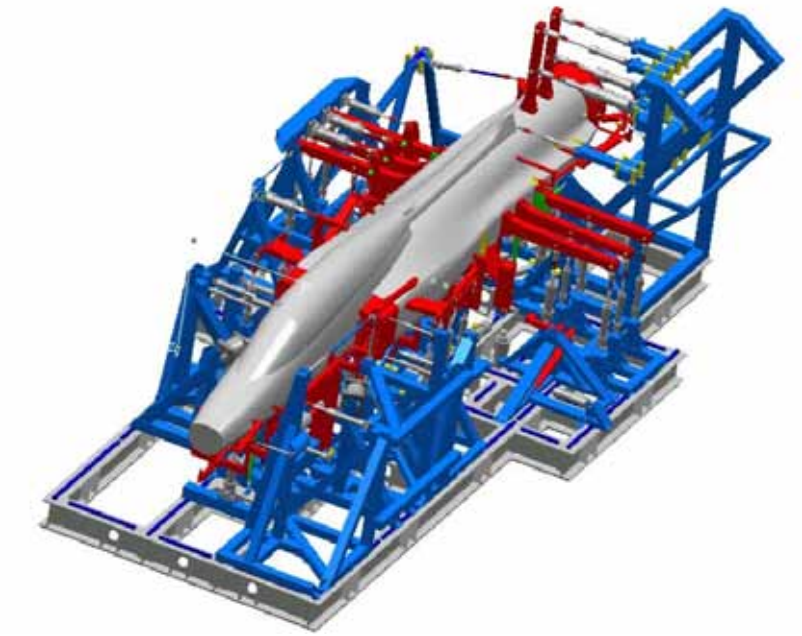

Figure 6. Schematic drawing of the full-scale test of Gripen twin-seater 39D.

Figure 7. Photograph of the forward fuselage, D version, with the air-to-air refuelling probe dummy.

The test is made in order to verify:

- Increased service life (8,000 flh)
- Changes due to part count reduction (e.g. introduction of high speed machined integral parts)
- Changes due to world wide climate adaptation (WWC)
- Increased cabin pressure
- Increased basic design mass
- Changes due to Air-to-Air Refuelling installation (AAR)
- Changes due to Radar Cross Section reduction (RCS)

A number of unit load cases and balanced load cases has been subjected to the test object before fatigue testing. The measured data have been used to certify new structures for full flight envelope. Some of the load cases will be measured after every 1,000 flight hour block of fatigue testing as well.

The repetition test sequence for the fatigue test consists of about 400 flights representing 500 flight hours. The goal is to exceed 32,000 flight hours of test simulation. The fatigue testing was started in January 2004 and has today (May 2005) reached 8,000 hours. A major inspection was done at 8,000 hours with no cracks detected except for a damage in the air-brake. This is handled separately while the testing is continued.

3.2.4 Load Spectrum Survey of Learjet LR-35

Saab Nyge Aero operates Mitsubishi MU-2 (twin turboprop) and Learjet LR-35 (twin jet) aircraft for special flight operations such as EW training and target towing. The operation of those aircraft differs from the operational profile they once was designed for and therefore requires special attention.

A load spectrum survey for the MU-2 aircraft has been running for a couple for years and show increased severity. The similarity in terms of operation between the two aircraft types calls for load spectrum survey also for LR-35.

An 8-channel MAS MICRO-II recorder system from SWIFT GmbH has been installed in one aircraft, figure 8. The system supports, besides one accelerometer for the cg load factor, 4 strain-gauge bridges in the wing on two spares and 3 strain-gauges in the horizontal stabilizer

1 Spar 7, Lower Skin, WS 21.5 Outboard of Splice Dblr
2 Lower Skin next to Spar 7, WS 31 Behind access Panel
3 Lower Dblr next to Spar 5, WS 7.2 Between Fuel Pump holes
4 Lower Skin next to Spar 5, WS 24 Outboard of Splice Dblr

5 Horiz Stab Fwd Upper Spar Cap BL 1.75
6 Horiz Stab Rear Upper Spar Cap BL 0.0
7 Horiz tail attach fitting, Near Vert Stab Spar 4
8 Normal Acceleration at CG, Nz

Locations of strain gauges in the wing are shown in figure 9.

Figure 8. Learjet LR35 aircraft.

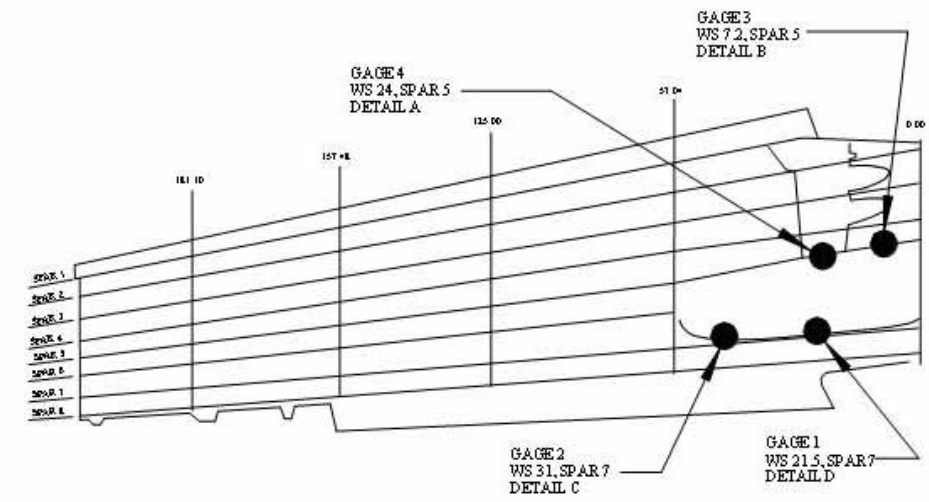

Figure 9. Locations of strain gauges in the wing.

A calibration flight was completed in January 2003 and recorded data, consisting of load factors and mechanical strains, was gathered during the period October 2003 to June 2004. The data recording equipment has been running during towing and jamming missions covering 110 flights and 169 flight hours. The measurement period has however not been sufficient long for a significant representation of the cyclic loading of the aircraft type in its specific operation. Instead, a synthetic composite spectrum has been defined together with the flight chief at Saab Nyge Aero using extracted missions from the measured data. These missions were combined to form 22 missions and a total anticipated annual usage of 400.9 hours. A typical time history from one wing strain-gauge is shown in Figure 10. The mission consists of four jamming flights.

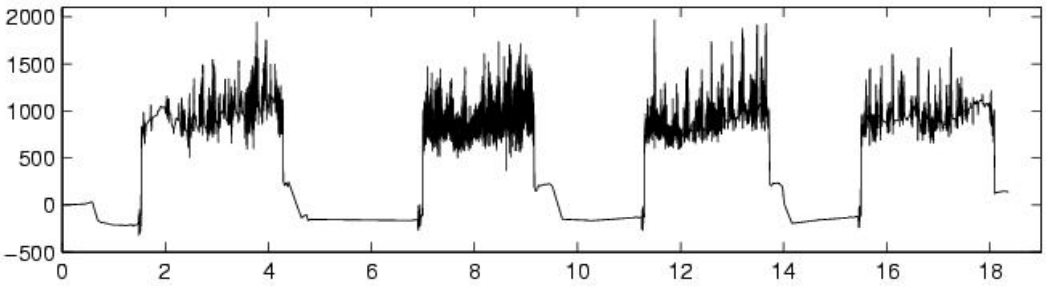

Figure 10. Typical wing strain time history versus hours for a jamming mission at low altitude covering four flights (ferry leg at beginning and end of first and last flight respectively).

Wing location 2 (Lower Skin next to Spar 7, WS 31) was the most severe location monitored.

The 400.9 flight hour stress spectrum for Location 2 is illustrated in Figure 11. The estimated design spectrum is also shown in this figure and shows that the target towing/jamming missions are substantially more severe for all alternating stresses above 5 ksi. These high stress cycles produce approximately 75% of the total damage.

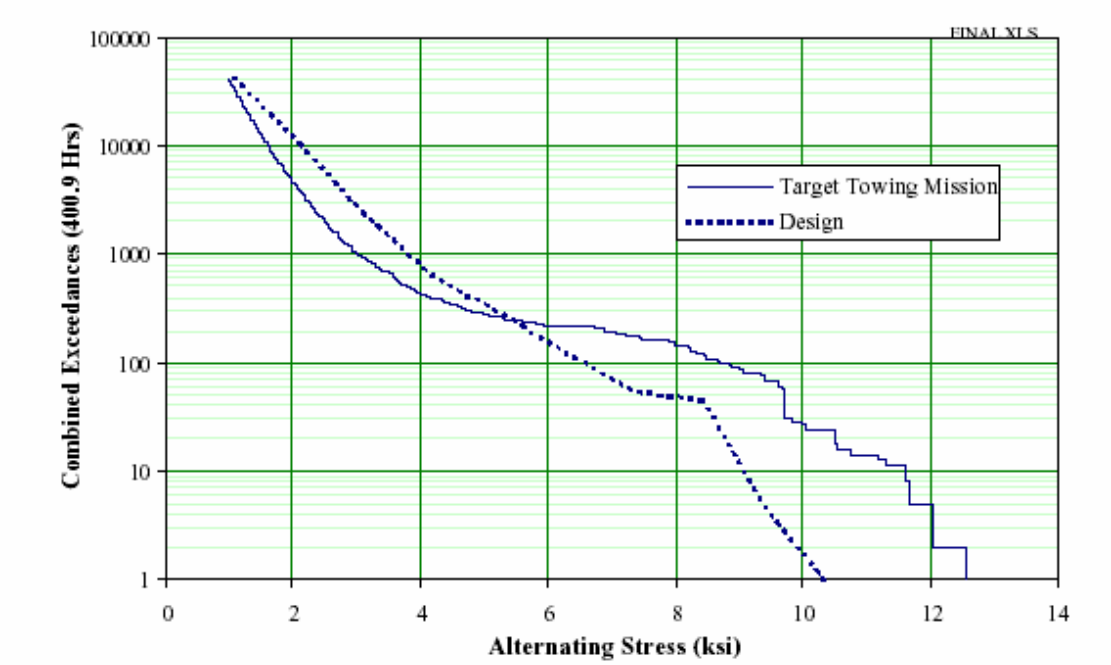

Figure 11. Comparison between design spectrum for LR-35 aircraft and measured wing spectrum.

Each mission was analyzed to determine the range-pair-range cycle counts and relative fatigue damage. The calculated fatigue damages were based on an aluminum S/N considered appropriate for the mean curve and are meant to provide relative mission severity and not to predict service lives. The damage rates between the most severe to least severe mission were found to vary by a factor of 68. Due to the varied missions in location, time of year flown, and flight profile; the data collected is not of sufficient sample size to make reliable conclusions about the stress spectrum over the monitored period much less projections about future spectra. Since the data indicates that the target towing/jamming missions are estimated to be four times more damaging than the design spectrum, continuing data recording will be done to ensure the spectrum is not under predicted.

The horizontal stabilizer and pivot fitting strains were also recorded and found to be small. The lives of the horizontal stabilizer and pivot fitting are not expected to be adversely affected by the target towing mission.

3.3 STRESS ANALYSIS AND FRACTURE MECHANICS

3.3.1 Direct Multiple Crack Fatigue Analysis of Large Built-up Structures

In fatigue analysis tabulated data for stress intensity factors are normally used. However, available data-bases cover mainly single cracks for a rather restricted parameter set and very simple geometries. In case of twin cracks of different sizes the situation is even worse. In the case of three or more cracks, a data base with stress intensity factors *K* for realistic parameter sets would become prohibitively large. By using the mathematical splitting scheme described in Ref. [1] stress intensity factors *K* can be effectively calculated as a part of the fatigue crack growth analysis also in case of multiple-crack configurations, Ref. [2].

A system for analysis of multiple crack fatigue growth was designed and tested on a large cluster of IBM computers made available through the US DoD HPC modernisation program. The present project is a joint project with US Air Force Academy in Colorado, U.S.A.. The objective was to demonstrate that this type of computations can be performed effectively and reliably on large computer systems having thousands of processors hence cutting computer time down to a minimum making advanced analysis of this type practically feasible. Computer systems having thousands of CPu's are becoming increasingly available in form of so called Linux-clusters.

The Splitting Method

The splitting scheme was the basic mathematical method used in the project, see Refs [2 - 4]. The method can be used to efficiently and reliably calculate the thousands of *K*-solutions needed for the various crack sizes needed in a single fatigue analysis, or, the millions of *K*-solutions needed in a statistical fatigue analysis, see Ref. [2]. A solid mathematical foundation is given in Ref. [1].

In the splitting method the problem is split into subproblems. The simple multi-site cracking scenario shown in Figure 12 (left part) is used to exemplify the decomposition of the problem of interest into global *un-cracked* problems and local problems with a single crack.

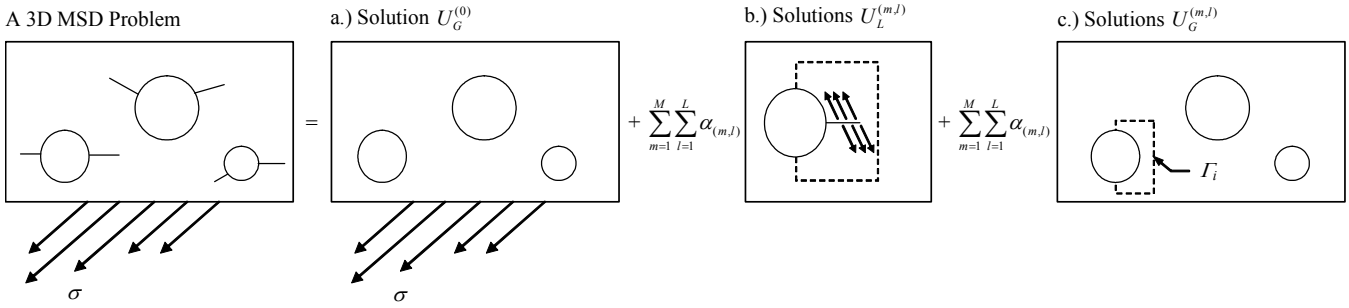

Figure 12. Principal sketch of splitting scheme sub-problems.

The three problems a, b, c (analysis levels I, III and V, respectively in Figure 12) are:

a. Global Crack Free Problem: The solution of the global crack free problem is $U_G^{(0)}$. This sub-problem is independent of the number and size of cracks under consideration, hence this very time consuming problem need be solved only once.

b. A Set of *M* Local Problems: A local model is developed for each crack size parameter and contact surface parameter (determined iteratively as a part of the global nonlinear solution [ICAF-review 2002/03]). The applied load consists of *L* different normalized crack surface tractions with the solutions denoted as $\left\{U_L^{(m,l)} \middle| m = 1, 2 \ldots M, l = 1, 2, \ldots L\right\}$. The local models contain a single crack.

c. A Set of Global Crack Free Problems: The global model in Figure 12a. is analyzed for prescribed *jumps* in tractions and displacements at the surfaces Γ_i used in the local problems. The solutions are denoted $\left\{U_G^{(m,l)} \middle| m = 1, 2 \ldots M, l = 1, 2, \ldots L\right\}$.

The approximate solution $\overline{U}$ to the exact 3D solution U is written as

$$\overline{U} = U_G^{(0)} + \sum_{m=1}^{M}\sum_{l=1}^{L} \alpha_{(m,l)} U_G^{(m,l)} - \sum_{m=1}^{M}\sum_{l=1}^{L} \alpha_{(m,l)} U_L^{(m,l)} \qquad (1)$$

where $\alpha_{(m,l)}$ are scaling factors determined by solving a small set of linear equations. The linear equations are obtained from the condition that crack surfaces shall be traction free. Thus with the known $U_G^{(0)}$, $U_G^{(m,l)}$, and $U_L^{(m,l)}$, the solution, $\overline{U}$ can be calculated with *virtually no computational cost per crack configuration*. This is very important when numerous solutions to the global problem are needed for different crack patterns. The computational efficiency of the strategy devised makes it feasible to perform Monte Carlo type studies of 3D multiple-site fatigue crack growth problems. We note that as L goes to infinity Eq. (1) is exact for arbitrary large non-planar cracks surfaces.

Figure 13a shows a small part of a fuselage shell analyzed in the project. The sub-mesh shown has 370 rivets and numerous possible 3D cracks. Figure 13b shows a local problem, of about 1000 problems considered, in the present study. Shells and rivets are modeled as three-dimensional objects. Note that fatigue crack growth of one, or, many (hundreds) of interacting cracks can be analyzed using the splitting scheme.

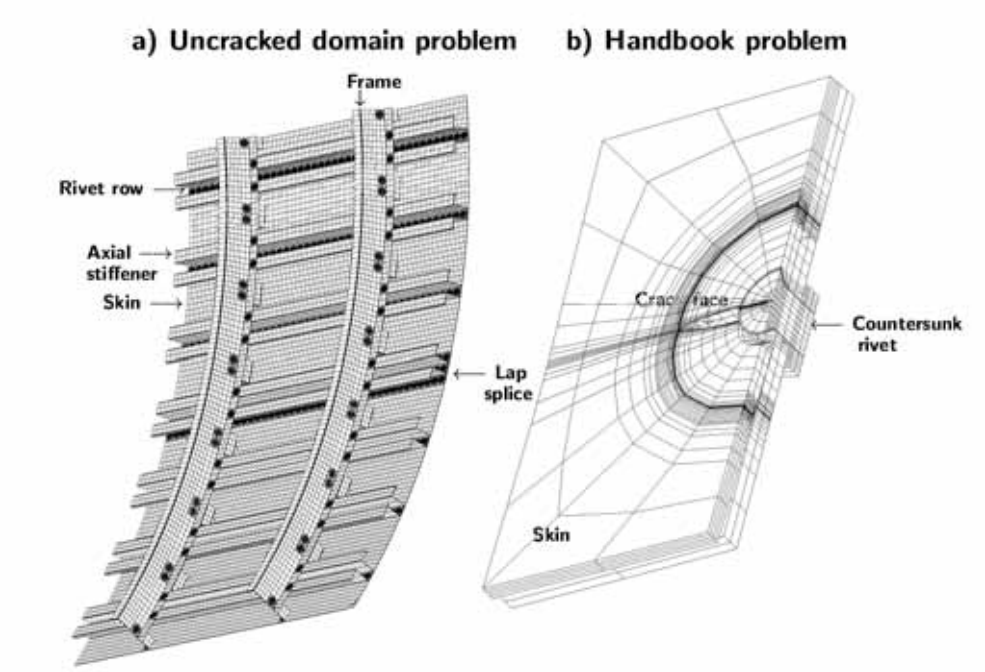

Figure 13. Part of fuselage shell without cracks (compare sub-problem a in Figure 12) and a typical local domain near a lap-splice with a 3D crack. Unknowns in the statistical nonlinear analysis are contact surfaces between the countersunk rivets and the plate.

The system Setup

The finite element program STRIPE used at levels I, III, V uses a *hp*-version of the finite element method and various novel mathematical methods, like the splitting scheme, to achieve scalability and computational efficiency. The costly part of the solution is to derive the local solutions $U_L^{(m,l)}$ (90-95% of cost) and the global solutions $U_G^{(m,l)}$ (5-10 % of cost), respectively (Equation 1). Computational characteristics of the different solution steps I, III and V are briefly summarized below.

Local solutions $U_L^{(m,l)}$

A typical computational domain is shown in Figure 13b. The contact problem between rivet-stiffeners-skin requires for its solution of the order of hundreds of thousands degrees of freedom for cases when a virtually exact solution is sought. Such computations are performed using typically 8 CPu's per local problem. Since local problems are uncoupled, perfect *scalability* is obtained, that is increasing the number of CPu's decreases the waiting time linearly.

Global solutions $U_G^{(m,l)}$

For multiple site fatigue analysis the domain shown in Figure 13a is in most cases sufficiently large. A high accuracy solution has less than 10^7 *DoFs*. The number of *DoFs* in the largest models we analysed in the project was $>10^8$. FE-models of this size allow a virtually exact numerical solution for arbitrary 3D crack patterns being derived as a part of the fatigue analysis. We remark that the largest models (with up to10^9 *DoFs*) are designed for future statistical residual strength analysis of fuselage and wing sections with multiple-site damage.

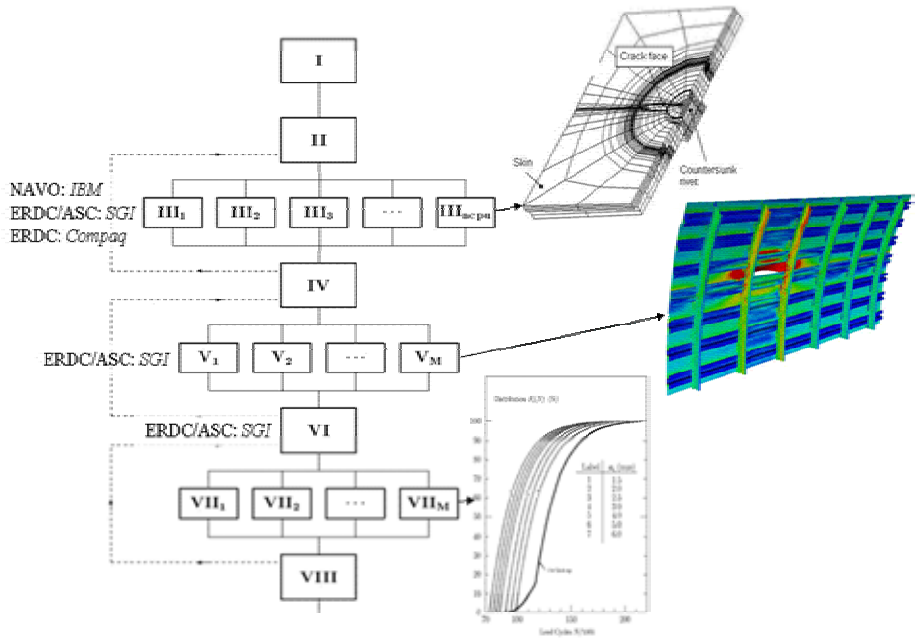

Figure 14. Schematic picture of splitting scheme for statistical analysis of built-up aircraft structures.

The approximate solution $\overline{U}$

The approximate solution $\overline{U}$ is obtained from (1). In fatigue analysis, equation 1 is used repeatedly where different solutions $U_G^{(m,l)}$ and $U_L^{(m,l)}$ corresponding to actual crack sizes and crack locations at time *t* are used. Such computations are performed on level VII, to negligible computational cost, and can be done in parallel for different crack scenario (statistical fatigue analysis).

Scalability

Figure 15 shows some scaling results obtained on a large IBM-computer when solving a large problem. Scalability curves shown are based on wall time. The systems I/O load was very high which explains the relatively low scalability numbers for level V jobs compared to level III jobs.

Figure 15 shows that the splitting scheme scales perfectly during the analysis of the local problems (level III). The global problem (level V) does not scale well above 256 CPu's due to extensive I/O. However, since the main part of the computational work is on level III, the computing time will be about 230 times shorter on a computer with 256 CPu's compared to computing on a single CPu computer.

Ageing Aircraft Analysis

The system shown in Figure 14 will also be used for statistical residual strength analysis of structures of the type shown in Figure 16. The results will be reported later.

The computational scheme will be used for fatigue and residual strength analysis of ageing US Military aircraft.

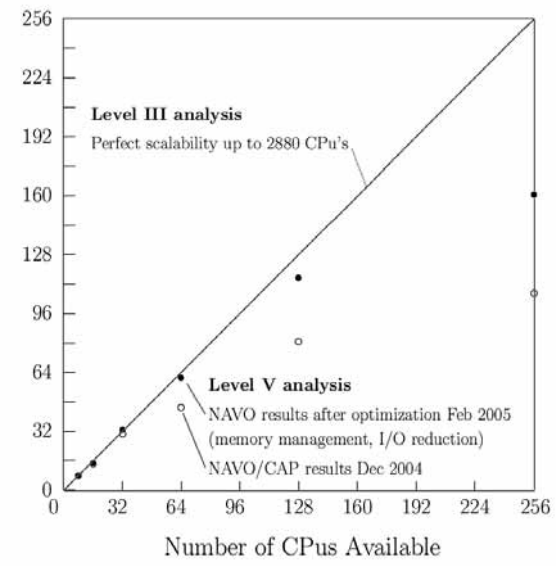

Figure 15. Scaling obtained at the NAVO/KRAKEN system, a 2944 processor IBM POWER4+ system operated by US DoD at Naval Oceanographic Office (NAVO) Major Shared Resource Center (MSRC).

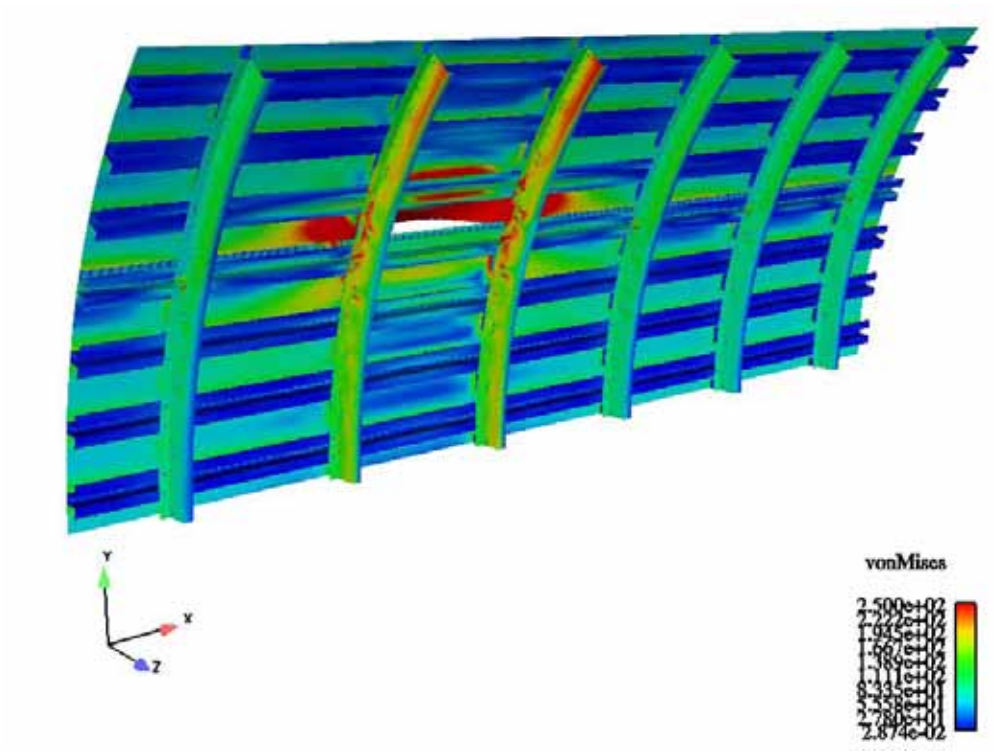

Figure 16. Fuselage section with a 500 mm long major crack and extensive *msd*-damage. A total of 1300 rivets, with potential fatigue damage, are considered in the statistical fatigue and residual strength analysis. FE-model consists of 700 000 solid elements.

3.3.2 A new method for fast and accurate *K*-calculation in case of very large irregular cracks in complex domains

The splitting method, Refs [1, 5], is a efficient and accurate method for calculation of stress intensity factors in case of multiple cracks in complex domains. The primary unknowns in the splitting scheme for calculation of stress intensity functions *K* are normal and shear tractions T_1, T_2, T_3 acting on crack faces on small sub-problems. Figure 17 shows schematically the decomposition of a fracture mechanics problem into global crack free problems and small local fracture mechanics problems (the problems with the

solutions $P_L^{(k)}$ in Figure 17). For cracks which are small, or of same size as local geometry dimensions (for example a hole diameter, Figure 17), the unknown tractions T_k can be well approximated by polynomials in the form,

$$T_k(r,z) \approx \sum_{i=0}^{p-1}\sum_{j=0}^{p-1} t_{ij}^{(k)} r^i z^j \qquad (2)$$

where $t_{ij}^{(k)}$ are unknowns in the discrete version of the splitting scheme *(r,z)* are coordinates in the (possibly curved) crack plane). For cases when cracks are very large compared to local structural dimensions, the crack surface stress distributions cannot be well approximated by low order polynomials (*p*=2-6, say) in the form of Eq. (2). Figure 18 shows a typical case where a relatively small part of a crack face is located in a region with a countersunc hole. For some parameter sets of interest in our case, say, *R/h*=0.075,*a/h*=0.6, *c/a*=10, we have *c/R*=80, that is the hole radius is very small compared to the crack size. For such cases the stress intensity function $K(\varphi)$ will be relatively smooth along the main part of the crack front and will blow up in a region near the countersunc hole. Figure 19, which shows the calculated (with the method described below) stress intensity function $K_I(\varphi)$ for remote tensile loading σ=1 and a plate width of 400*c* exemplifies this blowup. For nonregular crack faces the same principal difficulty exists and can be solved in the way described below.

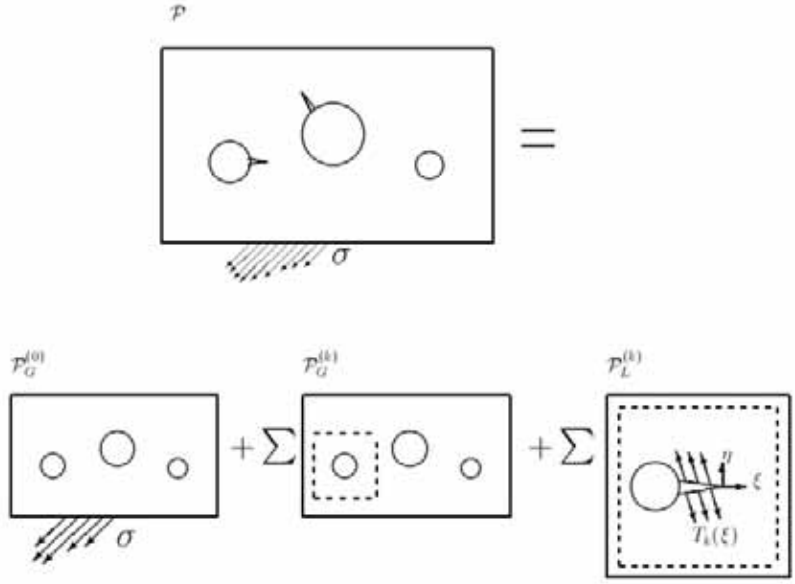

Figure 17. Decomposition of global problem *P* into two global crack free sub problems $P_G^{(0)}, P_G^{(k)}$ and small local problems $P_L^{(k)}$ with one crack, [1],[2]. Computational cost per crack configuration studied can be made very small since the global problem need not be reanalysed for each crack pattern of interest.

The splitting scheme described in Refs [1, 5] will converge also in case of *c/R* large but since high values of *p* must be used in Equation (2) this leads to prohibitive costs. To this end, in order to efficiently analyze problems with very large cracks, or problems with (large) irregular crack faces, a new version of the splitting method had to be developed. The idea is simply to approximate tractions $T_k(r,z)$ by piecewise polynomials defined on a one-dimensional radial ``mesh''. This ``mesh'' is defined by the radices $r_j, j = 0,1,...$ (Figure 18). The new traction approximation is,

$$T_k^{(hp)}(r,z) \approx \sum_{m=0}^{M}\sum_{n=0}^{p-1} v_{mn}^{(k)} N_m(r)\, z^n \qquad (3)$$

where $v_{mn}^{(k)}$ are coefficients to be determined.

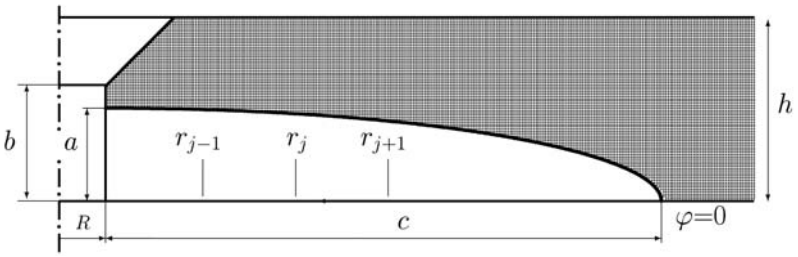

Figure 18. Crack with *c/R* ≈*12* near countersunk hole.

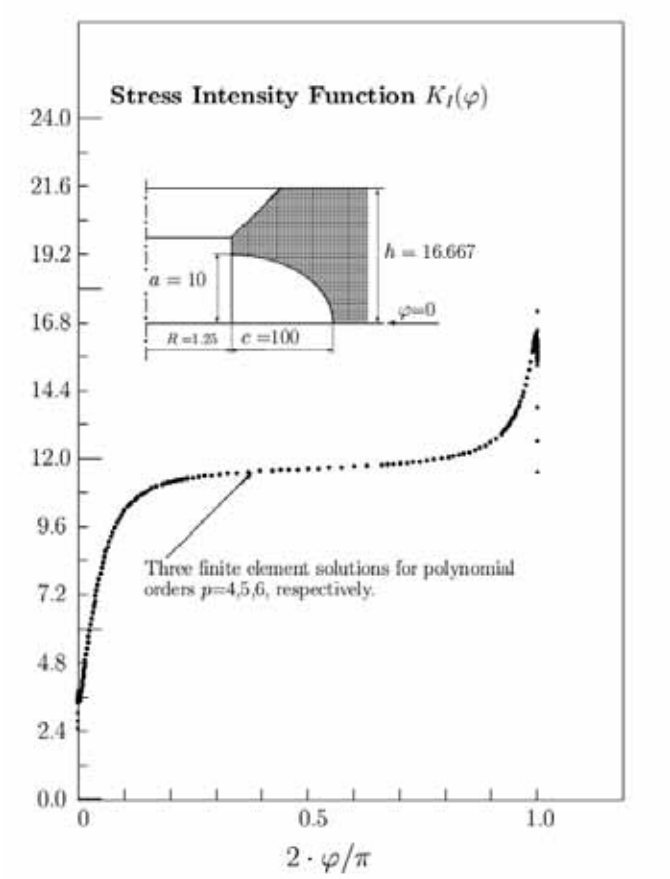

Figure 19. Variation of stress intensity factor $K_I(\varphi)$ for double crack at countersunk hole in plate subject to remote uniform tensile loading σ=1. Geometry parameters are *R/h*=0.075, *a/h*=0.6, *c/a*=10, *c/R*=80 with *R*=1.25. The three solutions shown are obtained using the *hp*-version of the splitting scheme where tractions are approximated by polynomials of order *p*=4,5,6, respectively. The three solutions are inseparable with actual resolution.

The functions $N_m(r)$ are polynomials, nonzero only in a local *r*-interval, as in the case of the standard *hp*-version of the finite element method. Hence, the functions $N_m(r)$ are identical to polynomials $P_m(r)$ defined on local *r*-intervals. Figure 20 shows the five lowest order functions $P_m(r)$ used in the present work.

The practical implementation of the *hp*-version of the splitting method is relatively straight forward. The steps indicated in Ref. [5] remains in principle the same, one difference is that the numerical integration have to be carried out over radial sections of the crack surface, where normal and shear tractions are applied

in the finite element analysis (local problems). Another difference is that some coefficient matrices needed have to be assembled in a way similar to the finite element analysis procedure. The finite element mesh of the local domain (Figure 17) must also have element edges corresponding to radices $r = r_j, j = 0,1,...$ in order to apply traction loading. Figure 21 shows a part of the 3D-mesh used to derive the data shown in Figure 19. Three radial elements (for the *hp*-splitting scheme analysis) with a grading factor 4 was used in the analysis, that is: $(r_{j+1} - r_j)/(r_j - r_{j-1}) = 4, j = 1,2,3$. Convergence tests on configurations with *c/R* ≈ 100 shows that the relative point wise error in $K_I(\varphi)$ is generally much lower than 10^{-3} polynomial order *p*=4 of the functions $N_m(r)$ and meshes of the type shown in Figure 21. Figure 19 exemplifies that the $K_I(\varphi)$-solutions for *p*=4,5,6 are inseparable with actual resolution (that is converged).

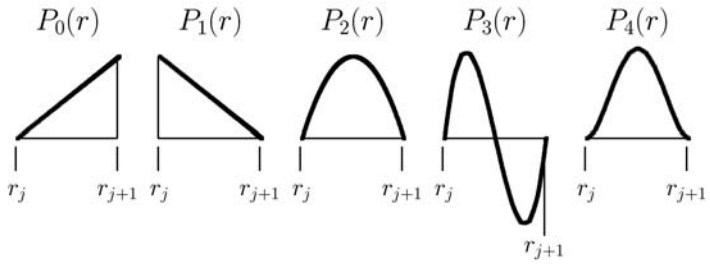

Figure 20. The lowest order basis functions $P_m(r)$ used to approximate $T_k^{(hp)}(r,z)$ in the *hp*-version of the splitting method.

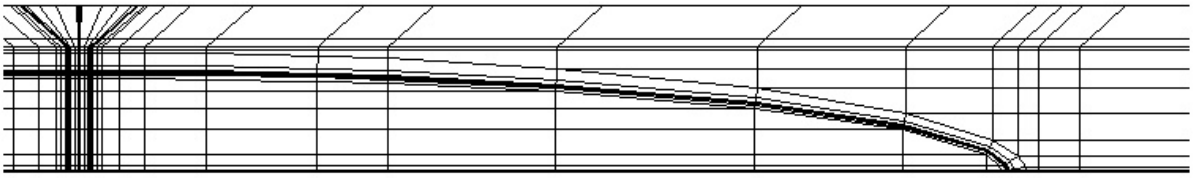

Figure 21. Part of mesh for *hp*-version of FEM and splitting method for large crack case with parameters *R/h*=0.075, *a/h*=0.6, *c/a*=10, *c/R*=80.

3.3.3 A large K data base

A very large stress intensity factor data base applicable to single and multiple cracks in basic structural elements is since 2002 being created in a joint project with United States Air Force. The data reviewed below will be available mid 2006. The data base will be implemented in the crack growth program AFGROW developed at United States Air Force. The number of crack geometries for which stress intensity factors are calculated are too numerous to list; however, they can be categorized as shown in Table 1 and in Figures 22 a-1d.

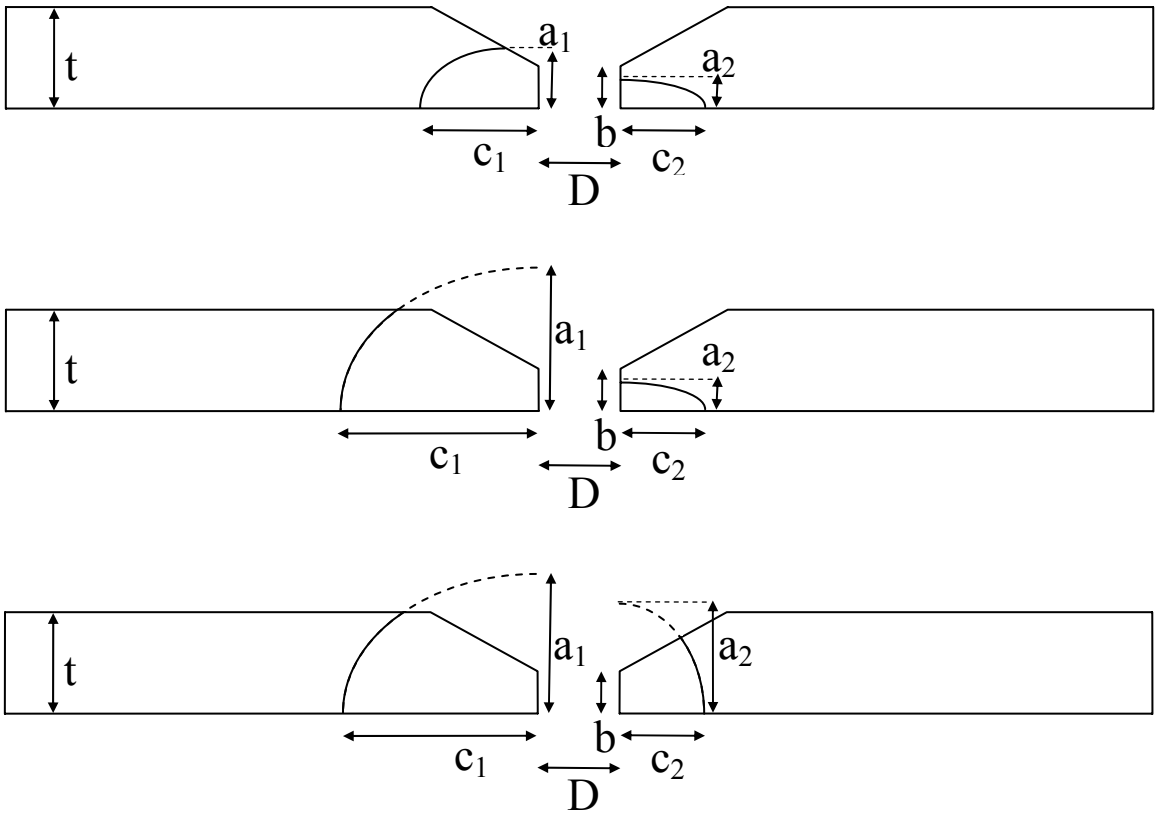

Figure 22a. Single or double cracks at countersunk hole

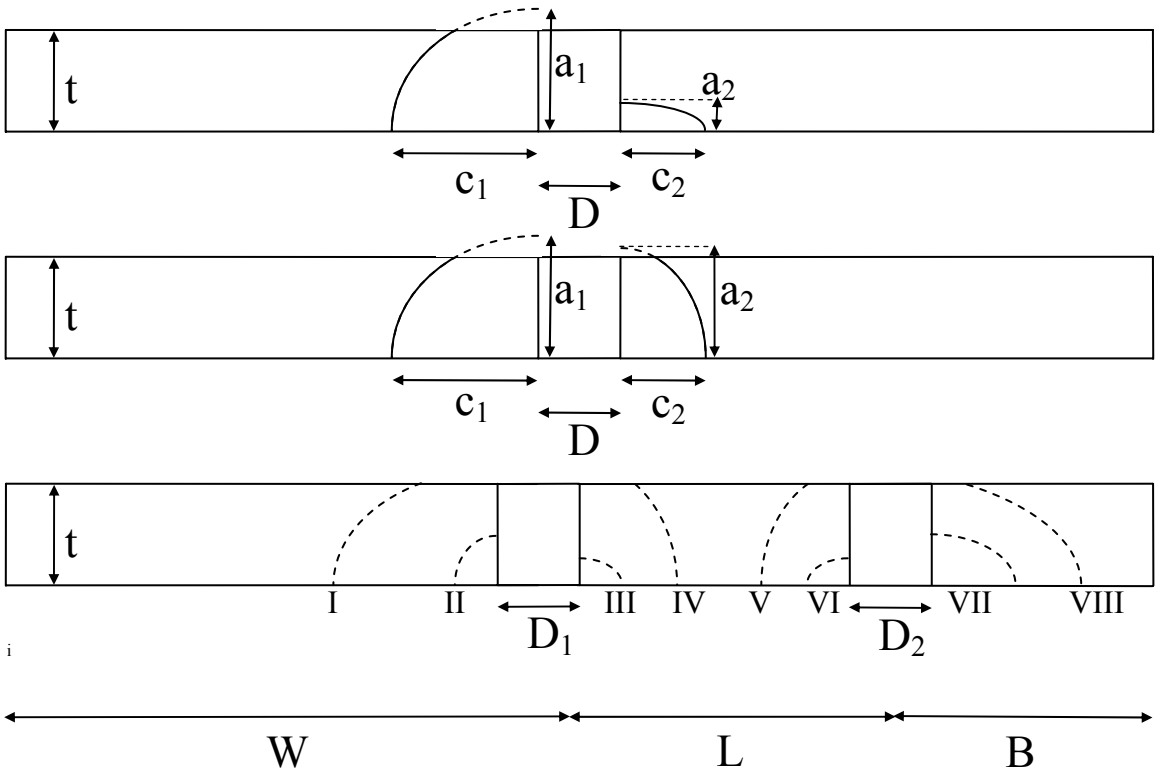

Figure 22. 1-4 cracks at straight shank hole(s).

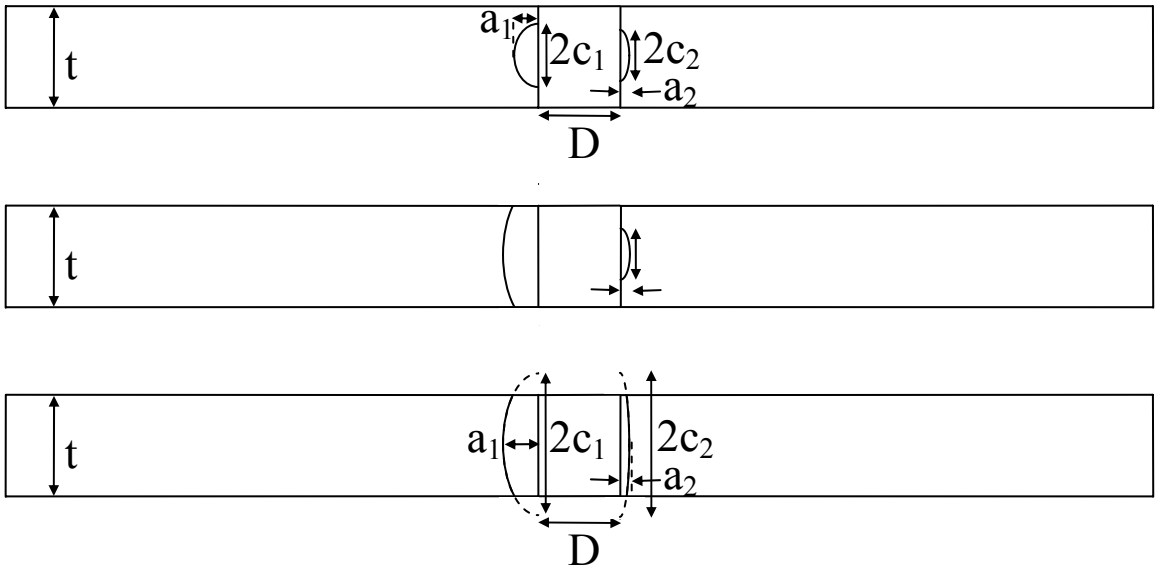

Figure 22c. Non-symmetric surface cracks at straight shank hole

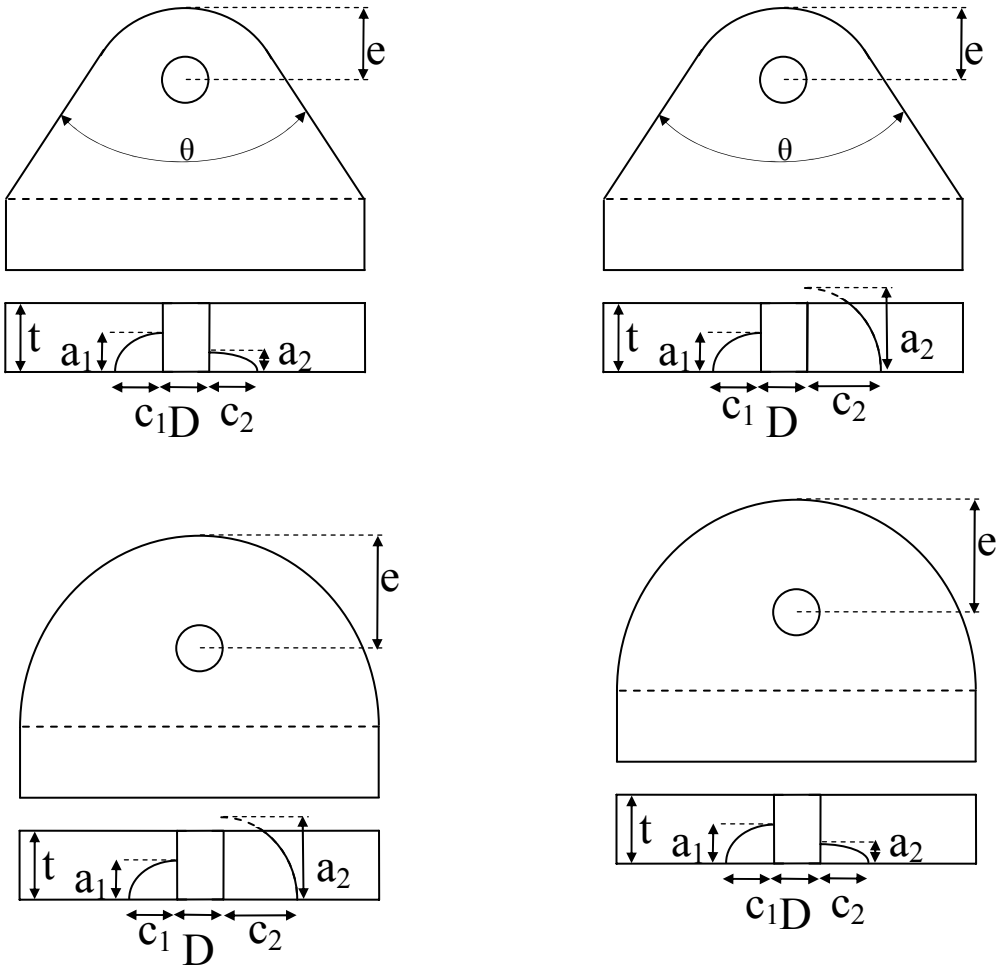

Figure 22d. Single or double cracks at lugs.

Figure 22 a – d. Structural elements and crack configurations analysed. In all 73 million single- and multiple-crack geometries are considered

Table 1. *K* Solution Parameter Space

Local Geometry	Hole Type		Crack Type		Loading			Number of *K* Geometries (Millions)
	Countersunk	Straight Shank	Part-Through the thickness	Through the thickness	Tension	Bending	Bearing	
Plate with Single Hole	1	1	1	1	1	1	1	29
Plate with Two Holes	1	1	1	1	1	1	1	39
Lug with Single Hole	1	0	1	1	1	1	1	5

The crack geometry is defined in terms of the local and crack dimensions; plate width, W, plate thickness, t, hole radius, r, hole diameter, D, countersink angle, θ, countersink depth, B, ligament spacing, L, crack depth, a, and crack length, c where,

Plate Geometry

r/t = 0.075, 0.1, 0.2, 0.333, 0.5, 1.0, 2.0, 3.0, 6.0
L = 1D, 2D, 3D, 4D where D is max(D_1, D_2) applies to two hole cases only
D_1/D_2 = 0.5, 1.0, 2.0 applies to two hole cases only
B = 1D_2, 2D_2, 3D_2, 4D_2

Part-Through Crack Geometry

a_i/c_i = 0.1, 0.125, 0.1667, 0.25, 0.5, 1.0, 2.0, 4.0, 6.0, 8.0, 10.0
a_i/t = 0.1, 0.2, 0.3, 0.4, 0.5, 0.6, 0.7, 0.8, 0.9, 0.95

Through Crack Geometry

a_i/c_i = 0.1, 0.125, 0.1667, 0.25, 0.5, 1.0, 2.0, 4.0, 6.0, 8.0, 10.0
a_i/t = 1.05, 1.5, 2, 3, 4, 5, 10

Hence, the structurally most significant crack shapes and loading conditions are considered. Table 1 shows for example that 39 million geometries are needed in order to cover the parameter set for the relatively simple twin hole geometry with 1-4 cracks shown in Figure 22b. An effective solution scheme for analysis of more general multi-crack situations in real-life structures is described in section 3.3.1.

The splitting scheme, section 3.3.2 is used to analyze the 73 million crack geometries with a guaranteed relative error less than 10^{-2} in stress intensity factors K_I, K_{II} and K_{III} along the entire crack front. Figure 23 exemplifies the principles behind mesh design for the hp-version of FEM which is considered in the design of the 86000 single-crack meshes needed, Ref. [5].

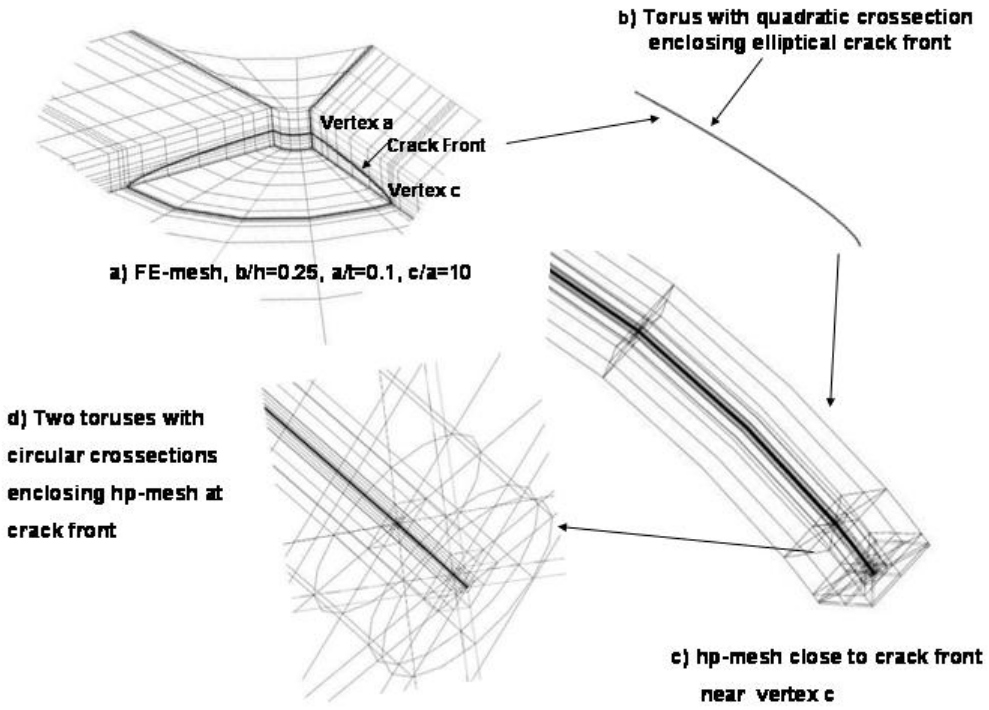

Figure 23. Meshes for the *hp*-version of FEM designed to capture the *K* distribution along the entire crack front, including the vertices. For *c/a* very large a special version of the splitting scheme is used.

3.4 FATIGUE CRACK INITIATION AND PROPAGATION

3.4.1 Effect of large plastic flow on the total fatigue life of metallic materials

Summary

One of the most important properties of metallic materials is their capability to tolerate large plastic deformation. Forging, stamping, rolling, and other production techniques may benefit from the plasticity of material. A less obvious aspect while being very important for the analysis of fatigue of metallic materials is the role of plasticity in the reduction of stress concentration in a complex structure. The local plastic yield reduces stress concentration so that high stress concentration may be tolerated. This aspect is seldom addressed when fatigue is considered. The yield may, however, lead to a different fatigue mechanism in the affected zone.

An investigation has been performed to evaluate the effect of large plastic deformation on the fatigue property of metallic materials. Fatigue tests have been performed under a constant amplitude loading condition with single notched specimens made of 2024-T3 aluminium sheets, both under original and plastic deformed condition, see Refs [6 - 7].

Fatigue Tests

The geometry of the specimen is shown in Fig.24a. This specimen is originally designed for the fatigue test of fastener joints to simulate various combinations of load transfer and secondary bending conditions. The sheet used in the tests has a thickness of 3.2 mm. A single notch is cut out on the side of the specimen to create a stress concentration location to limit where the fatigue crack may be initiated. The specimen is loaded along L-T orientation (the most fatigue resistant orientation). According to a boundary element analysis, this specimen has a stress concentration around 3.2 at the notch.

The specimens were produced according to the local workshop standard. There are no special treatments on the surface of notches for a smooth surface or to remove production damages and residual stresses.

For this specimen, fatigue cracks may be initiated either on the notch surface, or at the corner of the notch if there is secondary bending, see the insert in Fig.24a. The notch is cut using a cutting speed of 16 m/min and a feed speed of 2.5 mm/min. The diameter of the cutting tool is 5 mm. For plastically stretched specimens, the notch is cut after the specimen has been subjected a static load up to the desired deformation. Fatigue tests were then performed using MTS computer controlled hydraulic fatigue test machines. The fatigue test is controlled at a constant amplitude loading with a stress ratio of R=0.1.

The fatigue crack initiation and propagation is monitored using a measurement arrangement as shown in Fig.24b. In this arrangement, either laser speckle or white light is used to illuminate the critical area of the specimen (notch surface and one side of the specimen). During fatigue tests, two CCD cameras are used to follow the crack growth initiation and propagation process and to record images at pre-determined fatigue cycle intervals. The specimen is held statically when taking the images at a pre-determined load level.

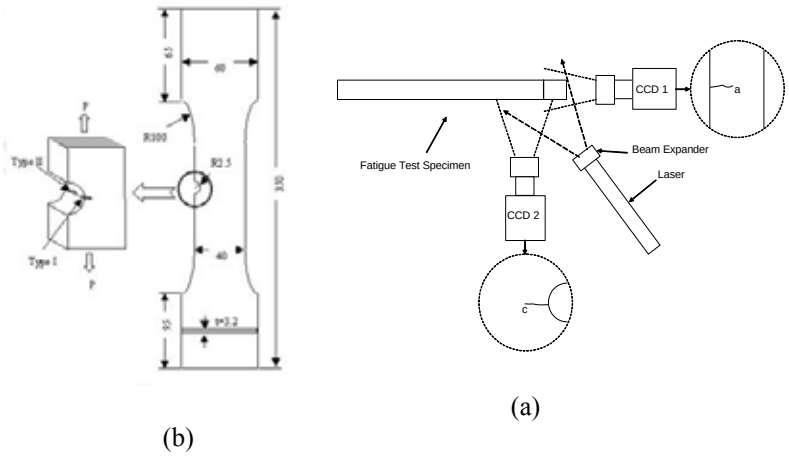

(a)

(b)

Figure 24. Fatigue test specimen and the arrangement to measure crack size.

After the specimen is broken, CCD images are analysed by comparing correlations between the image sequences to determine the size of crack and its propagation. A resolution of better than 0.1 mm is achieved using this technique for measurement of size of the crack.

The broken specimens were then inspected in both a microscope and a scanning electron microscope (SEM) to identify micro-mechanisms for the fatigue crack growth process, and to determine the effect of pre-plastic strain on the fatigue crack initiation and propagation.

Results and Discussions

Several static tests were performed to obtain the static mechanical parameters of the material. The static tests demonstrated that 2024-T3 has more than 18% plastic stretch before failure occurs. According to this result, 10% pre-stretch is used for the fatigue test specimens to investigate the effect of plastic deformation on fatigue life.

The reference fatigue test results show a close agreement with those results from AGARD small crack test results. The fatigue tests indicate that plastic deformation has effect on the fatigue life of material, depending on the load level. A reduction of more than 20% in fatigue strength has been observed near the fatigue limit regime while a less or no reduction at higher stress levels, see the comparison. The fractographic inspections indicate that plastic deformation may affect fatigue life through one of the mechanisms; the creation of a large number of micro cracks in the matrix of material, see Fig.25 c,d and Fig.26. As a result of the micro cracks, the crack initiation time is reduced and the fatigue life becomes shorter. The micro cracks created by plastic deformation also reduce the scatter in fatigue life.

Although there are indications that plastic deformation may affect crack growth rate, the tests showed that the crack growth rate is only marginally affected. The crack growth rate, derived from the curve fitting of the experimental crack size against load cycle, agrees well between the two different conditions, indicating the effect of plastic deformation on fatigue crack growth rate may be ignored in an engineering treatment. The difference in the total fatigue life may be mainly due to the crack initiation time.

Crack Initiation

The investigation indicates that different initial crack sizes may be needed in analysing the fatigue crack growth depending on the extent of gross plastic deformation, the stress level, and how many cracks may participate in the crack initiation process.

Various defects have been found on the surface of the material for both the pre-stretched and original sheets. However, the defects on the original material are dominated by various machine scratches and defects on material matrix as the micrographic images in Fig.225 a,b show. Fig.25a shows a typical machine scratch with the size of more than 10 μm . The defects due to particles impurities in material matrix are smaller than machine scratch as Fig.25b shows.

The surface condition is different after a large plastic stretch. Vast number of micro cracks in the size larger than 10 μm are created in the material matrix, see Fig.25c,d, both with the grains (Fig.25c) and along the grain boundaries (Fig.25d). Generally, the cracks formed within grain (Fig.25c) are much larger than those formed along the boundary of grain (Fig.25d).

Even though the defects on the original material surface have similar dimensions as the cracks formed after large plastic stretch, their roles on the crack initiation time are quite different.

A finite element analysis is performed to identify the crack initiation mechanism using finite geometrical and material non-linearity models in a commercial finite element code (ABAQUS 6.3). The analysis is concentrated especially on the large type of scratch as shown in Fig.25a.

Plane strain model was created to simulate the impact of an edged object on the surface of the material. The isotropic material model is assumed. The impact object is modeled as a rigid surface, with a high surface hardness than that of the base aluminum alloy. A half finite model was used due to the geometrical symmetry.

A six-step simulation was performed. The results are shown in Fig.27 for the results of opening stress (Model I) at the bottom of the scratch notch against simulation steps. The first step is to simulate the impact of a rigid edge with a round tip. The hard edge penetrates into the material, similar to the dent as shown in

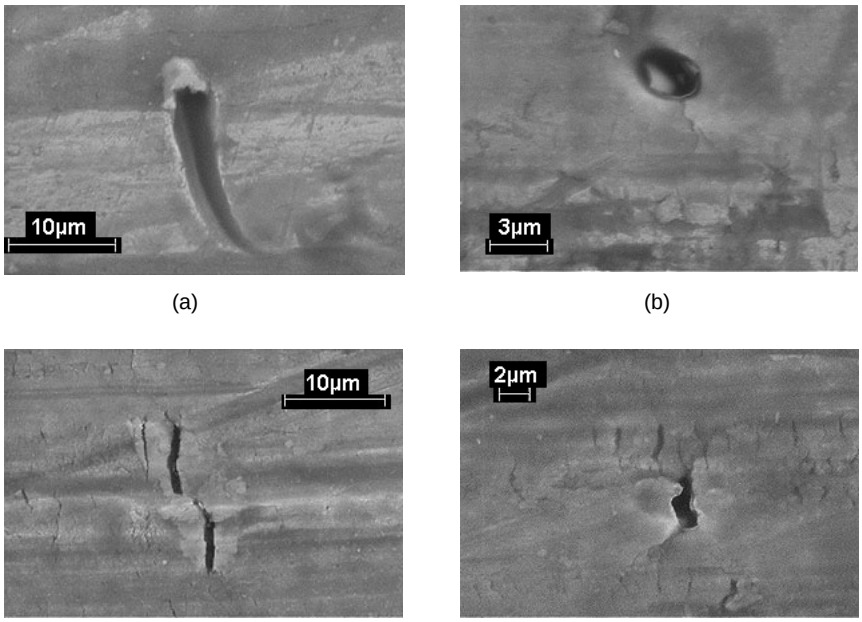

Figure 25. Microscopic surface condition of the specimens after 10% stretch.

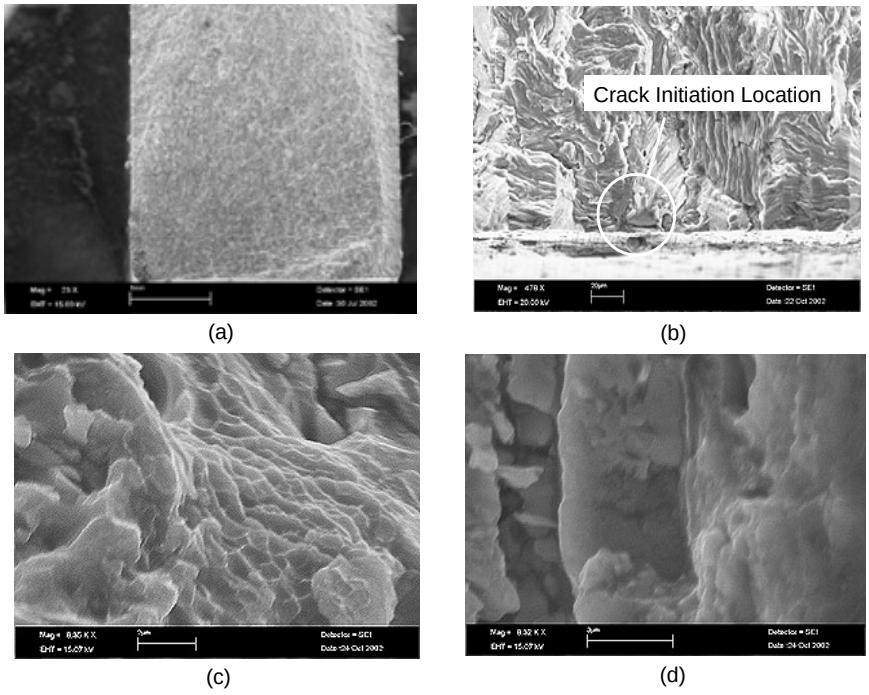

Figure 26. Comparison of fatigue (a-b) and static fracture (c-d) fractographic feature.

Fig.25a. Substantial compressive residual stress is created by this action when the edge is removed at step 2, leaving a dent on the surface of the material. The residual stress is at amplitude of -600 MPa, higher than the yield stress. This is due to the plane strain condition that has a two-dimensional stress state.

The significant residual stress makes will prevent crack initiation until the applied stress is more than 85% of initial yield stress (400 MPa). The strong residual stress exists at the bottom of the dent as well as on the side of the dent. When a fatigue load is applied, the residual stress state at the dent determines that fatigue crack can only be initiated at the other site of material instead of within the zone around the dent, see Fig.27.

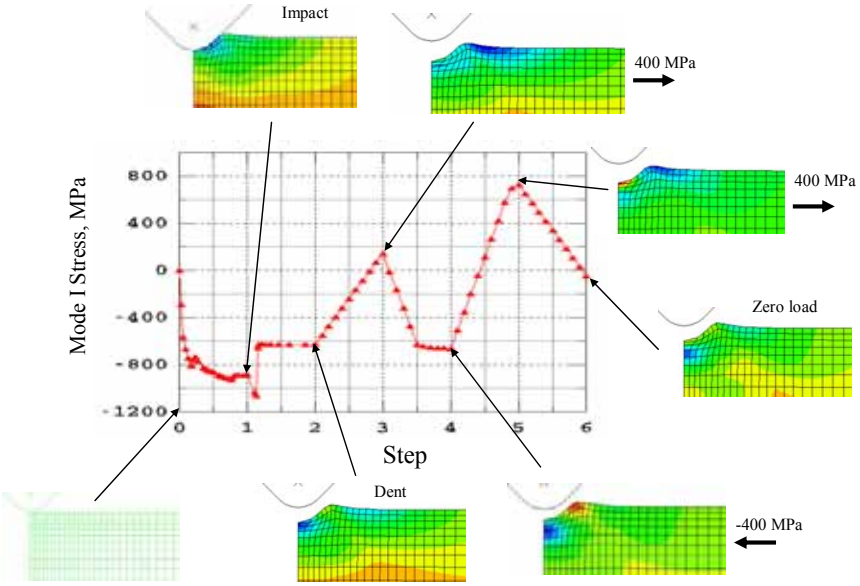

Figure 27. Schematic of the finite element simulation of the impact dent effect on the local stress condition.

The residual stress may be released with a significant compressive load, see Fig.27 for a compression of 400 MPa. The compressive plastic flow created by the stress concentration can release a large part of the compressive residual stress.

After the compression, for example, the residual stress on the bottom surface of the dent is reduced. However, the residual stress beneath the surface is still significant, creating a condition that a fatigue crack may be initiated on the bottom surface of the dent due to the stress concentration, but the crack has yet to overcome some resistant residual stress by penetrating a part of material before a fatigue crack is initiated. The crack may be stopped due to the residual stress.

The analysis gives a good explanation to the observation that fatigue cracks are initiated more often away from the machine scratches. Fig.28 shows a microscopic inspection at the notch of one specimen. In spite a significant number of machine scratches on the bottom of the notch, the fatigue crack is observed to be initiated away from the machine scratches in the material matrix on the part of smooth surface.

Accidentally, this analysis may also explain the difference between the reference test results and those of the tests performed under AGARD project. The specimens in AGARD test were prepared with a chemical process to remove a layer of material on the notch to remove the residual stress and machine scratches on the bottom of the notch. Probably, the beneficial effect of the machine scratches is removed as well so that the fatigue life becomes slightly shorter than that of the reference tests with original notch surface condition.

Conclusions

An investigation has been performed to evaluate the effect of plastic deformation on the fatigue property of metallic materials. Fatigue tests have been performed under the constant amplitude loading with single notched specimens made of 2024-T3 aluminium sheets, both under original and plastic deformed condition.

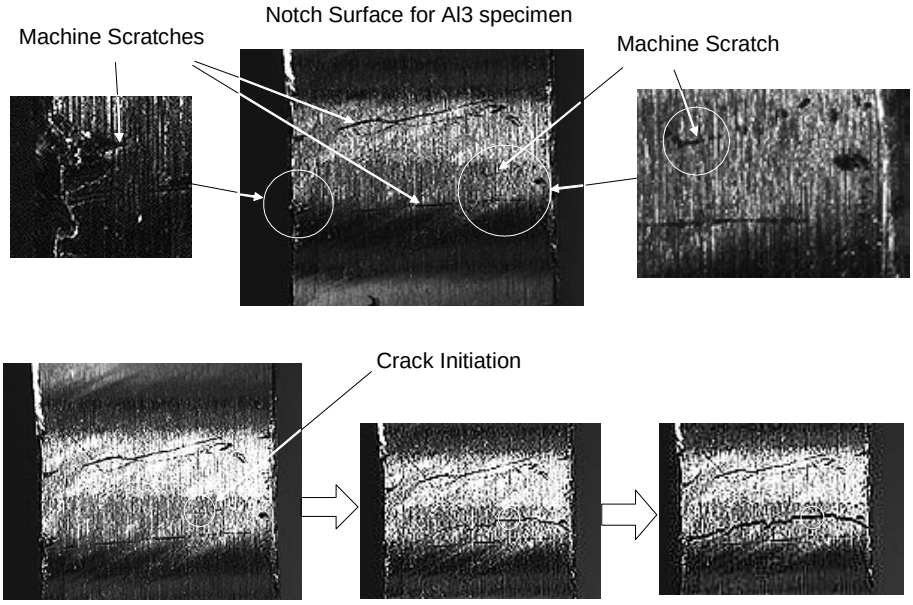

Figure 28. Site of the fatigue crack initiation.

The fatigue tests indicate that plastic deformation has a considerable effect on the fatigue life of material, depending on the stress level. A reduction of more than 20% in fatigue strength has been observed near fatigue limit while a less or no reduction may be expected at higher stress levels.

The crack initiation and propagation is monitored with either laser or white light illuminated CCD camera, and the fatigue crack growth is evaluated based on the image analyses. Microscopic and scanning electronic microscope inspections have been performed both on the specimen surface and on the fatigue and fracture surfaces to identify fatigue crack initiation and growth mechanisms for original as well as plastic deformed material.

The research shows that plastic deformation affects fatigue life through the creation of a large number of micro cracks in the material matrix. As a result, the crack initiation is accelerated and the fatigue life is reduced. The micro cracks created by plastic deformation also reduce considerably the scatter in fatigue life. Although there are indications that plastic deformation may affect the crack growth rate, the fatigue tests showed that the crack growth rate is only marginally affected, see Fig.29. In an engineering treatment, the effect of plastic deformation on fatigue crack growth rate may be ignored.

The investigation indicates that different initial crack sizes may be needed in analysing the fatigue crack growth depending on the stress level and how many cracks may participate in the crack initiation process.

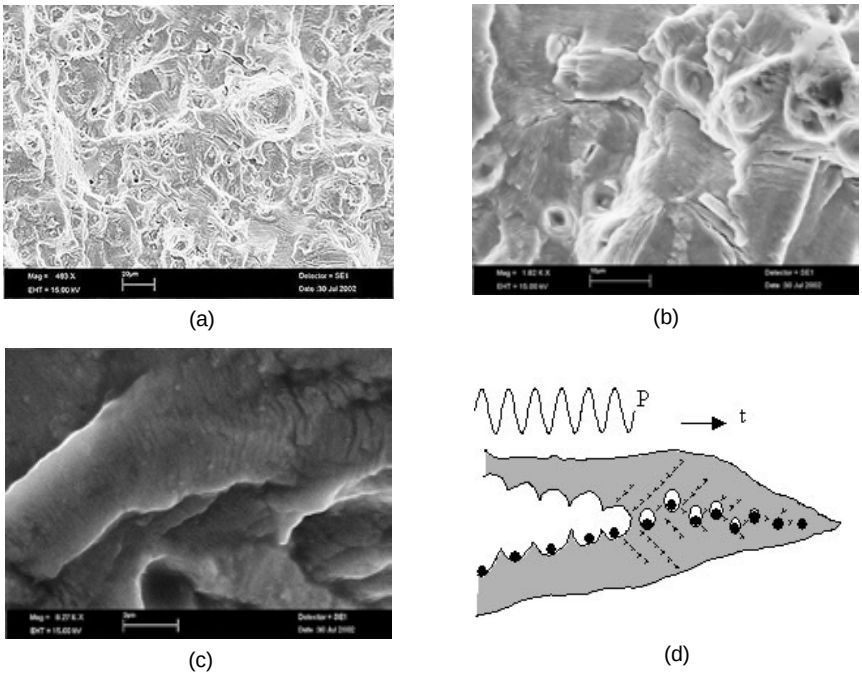

Figure 29. Fractographic of fatigue surface and simplified model of sub critical fatigue crack growth.

ACKNOWLEDGEMENTS

The work presented in this review was supported by the Defence Material Administration and Aging Aircraft Systems Squadron, Agile Combat Support Systems Wing, Aeronautical Systems Center, Wright-Patterson Air Force Base, OH, USA.

The assistance of Ms. Eva Norrbrand in preparing the manuscript is gratefully acknowledged. The editor is also indepted to the following individuals who helped to write parts of this review:

Börje Andersson	FOI	(Sections: 3.3.1, 3.3.2, 3.3.3)
Hans Ansell	Saab Aerosystems	(Sections: 3.2.3, 3.2.4)
Stefan Thuresson	Saab Aircraft	(Sections: 3.2.1, 3.2.2)
Geng-Sheng Wang	FOI	(Section: 3.4.1)

REFERENCES

1 Babuska I., Andersson B., The Splitting method as a tool for multiple damage analysis, SIAM J Sci Comp, Vol 26, No 4, 2005, pp 1114-1145.

2 Blom, A. F. (Ed) "A Review of Aeronautical Fatigue Investigations in Sweden during the period May 1997 to May 1999", FFA TN 1999-44 Stockholm 1999, 105 pp.

3 Blom, A. F. (Ed) "A Review of Aeronautical Fatigue Investigations in Sweden during the period May 1993 to April 1995", FFA TN 1995-13 Stockholm 1995, 94 pp.

4 Blom, A. F. (Ed) "A Review of Aeronautical Fatigue Investigations in Sweden during the period June 2001 to April 2003", FOI-R--0850--SE Stockholm 2003, 44 pp.

5 Fawaz S. A., Andersson B., Accurate stress intensity factor solutions for corner cracks at a hole, Engineering Fracture Mechanics 71,(2004), pp 1235-1254.

6 G. S. Wang, "Effect of local plastic stretch on total fatigue life evaluation", ECF 15, The 15th European Conference of Fracture, Stockholm, Sweden, August, 11-13, 2004, Stockholm, Sweden.

7 G. S. Wang and A. F. Blom, "Effect of large local plastic flow on the fatigue life of metallic materials", Proceeding of the 11th International Conference on Fracture, March 20-25, 2005, Turin, Italy, p. 562.